

# Open-Cell Aluminum Foams by the Sponge Replication Technique: A Starting Powder Particle Study

Alina Sutygina,\* Ulf Betke, and Michael Scheffler

Open-cell aluminum foams are manufactured by a sponge replication technique, and the effect of aluminum particles with different shapes and particle sizes on foam properties is studied. It is found that aluminum powder with spheroidal particles leads to aluminum foams with a lower strut porosity, a lower amount of alumina, and a higher compressive strength compared with foams manufactured from flaky, irregularly shaped aluminum powder. This effect is explained with the lower surface area of the first mentioned type of powder.

## 1. Introduction

Metal foams are cellular structures made of a solid metal containing large, mostly bubble-like gas pores inside. There are two types of foams: open cell and closed cell. In the closed-cell metal foams, pores are sealed within the solid metal. Open-cell foams have an interconnected network of pores. The most common properties of both types of metal foams are lightweight (porosity can achieve 98%) and possess electrical/thermal conductivity, nonflammability, a high-stiffness-to-weight ratio, and an energy/acoustic absorption.<sup>[1]</sup> Due to these properties, metal foams have found widespread applications in the aerospace industry, architecture, and automotive industry.<sup>[1,2]</sup>

Open-cell metal foams provide liquid/gas permeability additionally. Among the various metal foams, Al foams have received great attention due to low cost, the relatively easy manufacturing of required functional geometries, and better mechanical properties compared with other low melting metals. They are increasingly used in areas such as heat exchangers, filters, catalyst carriers, and electrodes in aluminum–air batteries where the combination of thermal/electrical conductivity and liquid/gas permeability is needed.<sup>[3–8]</sup> There is a variety of methods to produce open-cell aluminum foams such as investment casting, casting around hollow spheres, metal injection molding, and

space holder casting.<sup>[9–12]</sup> Despite widespread applications of these methods, there are disadvantages as a nonuniform cellular structure which depends on the shape of space holders and beads,<sup>[13]</sup> the relatively low specific surface area of foams, and high production cost.<sup>[10,13–15]</sup>

Nowadays, active research is currently under way to overcome these problems. Open-cell aluminum foams have been developed by a novel direct foaming process, in which an alkane phase and Al powder suspension were emulsified.<sup>[16]</sup> In that research, it was possible to adjust the porosity parameters of the foams via the properties emulsified suspensions. These foams possess high porosity (95–97%) with uniformly distributed, highly interconnected cells.


Another processing route to manufacture open-cell foams is the sponge replication technique, which is widely applied in the fabricating of open-celled ceramic foams.<sup>[17,18]</sup> The sponge replication technique was established by Schwartzwalder et al.<sup>[19]</sup> This technique is widely applied in the fabrication of ceramic foams, and it allows to obtain high porosity. This process is less complex to carry out with its three production steps. First, a polyurethane (PU) sponge or template is coated with a slurry. The next step is the thermal removal of the PU templates. Finally, the foam is thermally treated.

The obtained structure replicates the shape of the PU template. The manufactured foams are characterized by a uniform cellular structure, high specific surface area, controllable pore size, and porosity  $\geq 90\%$ , and high liquid/gas permeability due to high open-cell porosity.<sup>[20,21]</sup> In addition, the sponge replication technique increases the open strut porosity due to hollow struts, when compared with other manufacturing processes. The combination of the aforementioned properties is attractive for applications of aluminum foams as catalyst carriers or filters.

The sponge replication technique has been used for the manufacturing of open-cell titanium,<sup>[22,23]</sup> Cu, and Ti<sub>6</sub>Al<sub>4</sub>V foams<sup>[24,25]</sup> and also to produce open-cell aluminum foam.<sup>[26,27]</sup> In a study by Zaman and Keleş,<sup>[26]</sup> the determination of the slurry composition was mainly focused upon, samples were heat treated only in air at 620 °C for 4 and 7 h. The porosity levels were found in a range of 94.4–95.5%. In the study by Yagsi and Keleş,<sup>[27]</sup> the fabrication of open-cell aluminum alloy foams in the argon–vacuum atmosphere at 1050 °C was investigated. However, the sponge replication technique was not developed any further for the preparation of aluminum foams.

The aim of this work is to demonstrate the feasibility of Al foam manufacturing with the sponge replica process using

A. Sutygina, Dr. U. Betke, Prof. M. Scheffler  
Institute for Materials and Joining Technology – Nonmetallic Materials  
Otto-von-Guericke-University Magdeburg  
Große Steinernetischstraße 6, 39104 Magdeburg, Germany  
E-mail: alina.sutygina@ovgu.de

 The ORCID identification number(s) for the author(s) of this article can be found under <https://doi.org/10.1002/adem.201901194>.

© 2020 The Authors. Published by WILEY-VCH Verlag GmbH & Co. KGaA, Weinheim. This is an open access article under the terms of the Creative Commons Attribution License, which permits use, distribution and reproduction in any medium, provided the original work is properly cited.

DOI: 10.1002/adem.201901194

an aqueous aluminum slurry as the starting material system and heat treatment in a vacuum.

## 2. Experimental Section

### 2.1. Specimen Preparation

In this work, two types of aluminum powders were used: 1) air-atomized aluminum powder supplied by Ecka Granules (MEP103 RE903, Ecke Granules, Ranshofen, Austria) with 99.5% purity and an average particle size  $<10\ \mu\text{m}$  and 2) Aldrich Aluminum 11010-250G-R (Aldrich Chemie GmbH, Steinheim/Germany) with a particle size of  $\approx 90\% \geq 45\ \mu\text{m}$ .

For the preparation of the samples, the aluminum powders, distilled water, a polyvinyl alcohol binder (1.2 wt%, Optapix PA 4G, Zschimmer& Schwarz Chemie GmbH, Lahnstein, Germany), and an open-cell PU template with a linear cell count of 20 ppi and a geometric size of  $20\ \text{mm} \times 20\ \text{mm} \times 20\ \text{mm}$  (Koepp Schaum GmbH, Oestrich-Winkel, Germany) were used. Polyvinyl alcohol was dissolved in distilled water under continuous stirring until a binder content of 10.7 wt% was reached. Then, the aluminum powder was added into the binder/water solution. The mixtures were stirred with a stirring rate of 2000 rpm for 6 min using a planetary centrifugal mixer (THINKY Mixer ARE-250, THINKY Corp. Tokyo, Japan) and cooled to room temperature as the temperature increased during mixing. The dispersions composition and heat-treatment conditions are shown in **Table 1**.

The PU foam was used as a template, which was dipped into the corresponding dispersions, and excess dispersion was removed by air blowing. Then the samples were dried for 24 h at room temperature. The binder and PU burning out were conducted in air at  $250\ ^\circ\text{C}$  for 3 h and at  $500\ ^\circ\text{C}$  for 3 h in a circulating air furnace (KU 40/ 04/A, THERMCONCEPT Dr. Fischer GmbH, Bremen, Germany). The final heat-treatment step was at  $750\ ^\circ\text{C}$  for 3 h in vacuum atmosphere ( $1.2 \times 10^3\ \text{Pa}$ ). The heat-treatment step was conducted in a conventional tube furnace (alumina tube, HTRH 70-600/1800, Carbolite-Gero GmbH & Co. KG, Neuhausen, Germany). The heating and cooling rates were  $3\ \text{K min}^{-1}$ . **Figure 1** shows schematically the sample preparation.

**Table 1.** Dispersion composition and heat-treatment conditions used for the manufacturing of the Al foams.

Powder	Al powder [wt.%]	Binder burning		PU burning		Heat treatment	
		T [ $^\circ\text{C}$ ]	Time [h]	T [ $^\circ\text{C}$ ]	Time [h]	T [ $^\circ\text{C}$ ]	Time [h]
Aldrich	57	250	3	500	3	750	3
Ecka	70.6						

### 2.2. Characterization

The powder morphology and the microstructure of cross sections of the heat-treated Al foams were characterized by scanning electron microscopy (SEM; FEI ESEM XL30 FEG, Hillsboro, USA). The foams were vacuum impregnated in epoxy resin and were ground (180, 320, 600, 800, 1200, 2500, and 4000 mesh grinding paper) and polished (diamond suspension  $3\ \mu\text{m}$  and  $1\ \mu\text{m}$ ). A Hydro 2000SM (Malvern Instruments, Malvern, UK) particle-size analyzer was used for the measurements of the particle size distribution of the powders.

Differential scanning calorimetry (DSC) and thermogravimetry (TG) were used to analyze the thermal transformation with respect to weight change and oxidation onset of powders. DSC and TG were conducted with the thermal analyzer STA 449 F3 Jupiter (Netzsch-Gerätebau GmbH, Selb, Germany) in air with a flow rate of  $50\ \text{mL min}^{-1}$  and a heating rate of  $10\ \text{K min}^{-1}$  from room temperature to  $800\ ^\circ\text{C}$ .

The characterization of the foam's macrostructure micro-computed tomography ( $\mu\text{-CT}$ ) was conducted by a nanotom S tomograph (Phoenix/GE Sensing & Inspection, Wunstorf, Germany). The voxel size of the measured foams was  $6.5\ \mu\text{m}^3$ , there was a set of 1080 radiographs with a resolution of  $2304 \times 2304$  pixels, and an exposure time of 1250 ms per image. The Phoenix Datos I X 2.0 software package (Phoenix/GE Sensing & Inspection) and the CTAnalyser 1.17 software package (CTAn, Skyscan/Bruker microCT, Kontich, Belgium) were used for data acquisition, reconstruction, and the calculation of the cell sizes and strut thickness, respectively. The CT data import into the CTAn software and the actual morphological calculations of the differential thresholding-based binarization procedures are described in detail in a study by Betke et al.<sup>[28]</sup> The hollow struts were filled before the calculations of the cell size and strut thickness distributions. This step was performed with a morphological closing operation in CTAn with a round kernel,  $r = 13\ \mu\text{m}$ .<sup>[29]</sup>

X-ray diffraction (XRD) analysis was conducted by an X'Pert Pro diffractometer (PANalytical GmbH, Kassel, Germany,  $\text{Co K}\alpha^{1/2}$  radiation,  $2\theta$ ,  $40^\circ\text{--}85^\circ$ ) with Bragg–Brentano geometry. The Topas Academic V5 software package was used to determine the phase composition in the supplied powders and the thermally processed foams with the Rietveld analysis.<sup>[30]</sup>

The total porosity was measured based on the relation  $P_{\text{total}} = 100 \cdot (1 - \rho/\rho_0)$ ,<sup>[31]</sup> where  $\rho_0$  is the density of aluminum ( $2.7\ \text{g cm}^{-3}$ ), and  $\rho$  is the density of the obtained foams. The open porosity of the heat-treated foams was quantified by the Archimedes method, using water as the infiltrating fluid according to the DIN EN 623-2:1993-11 standard procedure.<sup>[32]</sup> Due to the complex geometry of the aluminum forms, residual water

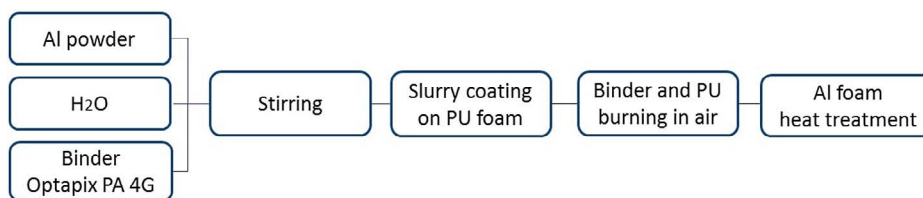


**Figure 1.** Schematic illustration of the samples preparation.

remains within the strut cavities formed after the PU burnout. According to the DIN standard, water adhering superficially to the sample has to be removed. To solve this problem, the volume of the PU foam struts was subtracted from the total strut pore volume.<sup>[33]</sup> This value was calculated from the average template weight of 1.52 g for a 50 cm<sup>3</sup> foam piece and a PU skeletal density of 1.1 g cm<sup>-3</sup>, according to He pycnometry. In this way, the volumes of the cavities after PU burnout were corrected by the volumetric shrinkage of the heat-treated foams.

Compressive tests were conducted with a TIRAtest 2825 mechanical testing machine (TIRA GmbH, Schalkau, Germany). The load was set to 2 mm min<sup>-1</sup>, and ten specimens were used for each test. The software Visual-XSel 14.0 (CRGRAPH, Starnberg, Germany) was used for the calculation of the Weibull modulus and Weibull parameter *m* for the compressive strength to each sample and sample series, respectively.

### 3. Results and Discussion

Figure 2 shows the SEM images of the aluminum powders and the particle-size distributions of both types of powders. The Aldrich powder has a flaky, irregularly shape and some cracks can be seen on the surface (Figure 2a). The Ecka powder has a smooth surface and is of spheroidal geometry. The Aldrich powder is characterized by  $d_{50} = 16.6 \pm 0.8 \mu\text{m}$  with 10% < 5.0  $\mu\text{m}$  and 10% > 51.8  $\mu\text{m}$ . For the Ecka powder,  $d_{50} = 6.2 \pm 0.3 \mu\text{m}$ , with 10% < 2.7  $\mu\text{m}$  and 10% > 13.4  $\mu\text{m}$ .

The TG and DSC curves of the aluminum powders are shown in Figure 3. The mass loss of the powders below 400 °C is mainly

caused by the desorption of gaseous species and water vapor and other airborne species adsorbed on the surface of the powder. From the DSC results, it follows that each powder shows an exothermic oxidation reaction and a subsequent endothermic melting process. The onset temperatures of the exothermic oxidation peak for the flaky, irregularly shaped Aldrich powder are  $\approx 586$  and  $\approx 580$  °C for the spheroidal-shaped Ecka powder. The melting peaks are located at  $T_{\text{mAl}} = 660$  °C for the Aldrich and  $T_{\text{mAl}} = 665$  °C for the Ecka powder. The difference in the melting peak temperatures might be associated with a small amount of titanium (<0.25 wt. %) in the Ecka powder; the melting temperature of plain Al is  $T_{\text{m}} = 660$  °C.<sup>[34]</sup>

There is a continuous weight gain after the start of the oxidation reaction (Figure 3). The rate of the weight gain decreases with the onset of the endothermic reaction on both powders. Despite this, the weight gain of Aldrich powder after the onset of the endothermic melting process is more intense in comparison with that of the Ecka powder. The total weight gain at 750 °C is 18 wt% for Aldrich powder and 3 wt% for Ecka powder.

From the results mentioned earlier, it can be concluded that the oxidation rate is not only related to the particle size—due to a larger surface area with smaller particles, the oxidation rate—with mass gain as a measure—should be higher compared with that of larger particles—but is also related to the shape of the particles. Therefore, the larger but irregularly shaped particles in the Aldrich aluminum powder form more aluminum oxides during the TG experiment.

Figure 4 and 5 shows the SEM images of cut struts and cross sections of the Al foams heat treated at 750 °C for 3 h. The struts are hollow, as to be expected from the manufacturing process.

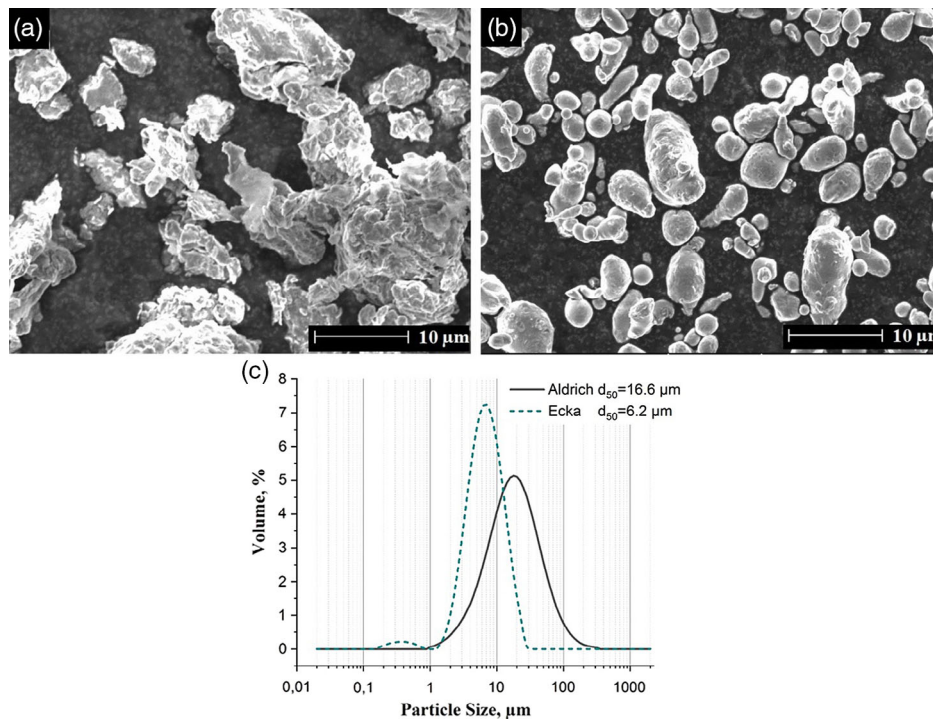


**Figure 2.** SEM images of the a) flaky, irregularly shaped Aldrich and b) dendritic near-spherical-shaped Ecka powders; c) particle-size distributions of the Aldrich and Ecka powders.

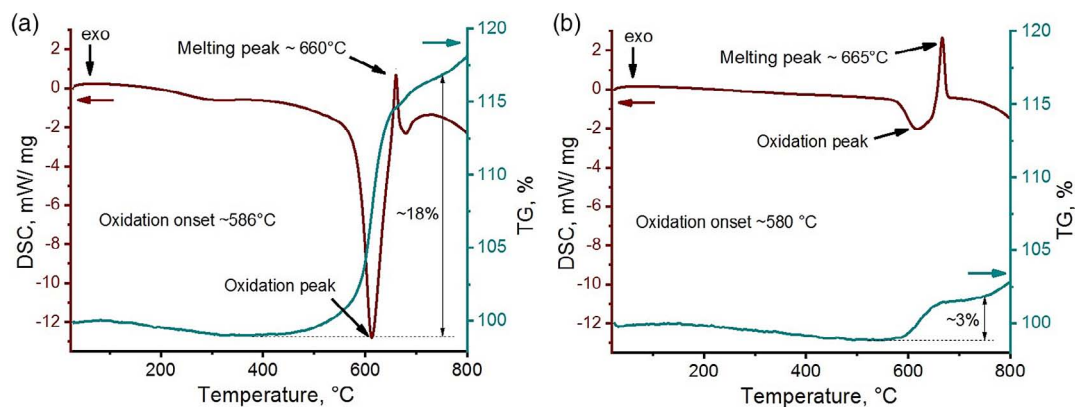


**Figure 3.** TG and DSC curves of the a) flaky, irregularly shaped Aldrich and b) spheroidal Ecka powders.

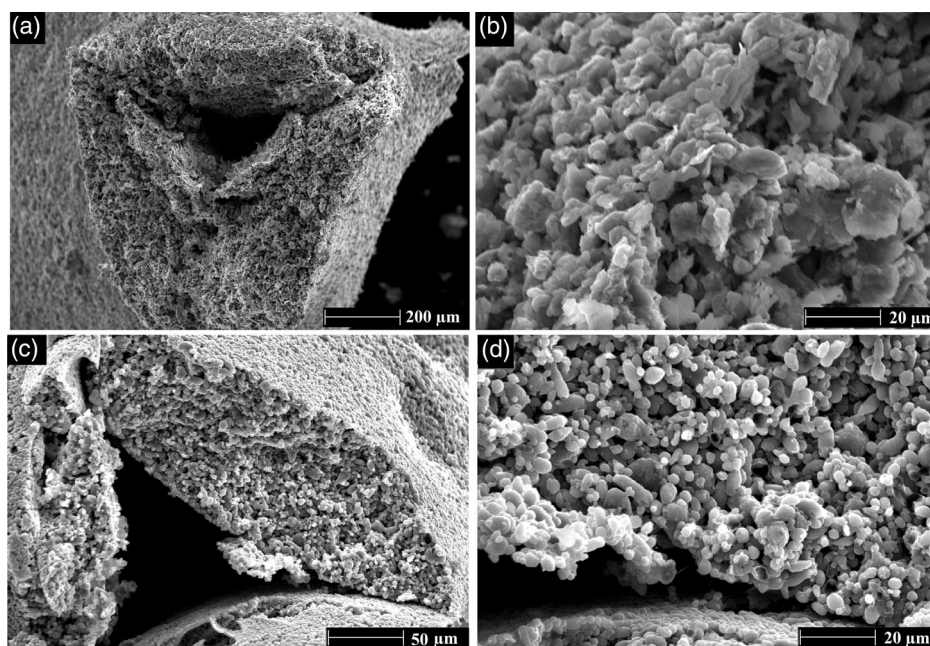


**Figure 4.** SEM images of cut struts of the foams made from the a,b) flaky, irregularly shaped Aldrich powder and c,d) spheroidal-shaped Ecka powder after heat treatment at 750 °C for 3 h.

The cavities in the struts are the result of the replication process of PU foams. However, the foams made from the spheroidal-shaped Ecka powder are characterized by the presence of molten aluminum beads outside the struts (Figure 5c). Simultaneously, there are cracks along the strut walls for the foams manufactured from the flaky, irregularly shaped powder (Figure 5a). The cut struts and cross section of both foams are porous with non-uniform structures of foam struts. This is related to incomplete heat treatment due to the existence of a thin oxide layer on the powder surface;<sup>[35,36]</sup> for the oxide layer disruption, an additional processing step may be implemented in a forthcoming work.

The strut cross section of the foams made from the spheroidal-shaped Ecka powder consists of a fine-grained structure in comparison with the foams manufactured from the flaky, irregularly shaped Aldrich powder. After heat treatment of the powder,

particles of the foams made from the Ecka powder are more connected to each other, forming conglomerations of formerly molten powder particles, unlike the foams made from the Aldrich powder. Therefore, the foams made from the Ecka powder are characterized by a comparatively densely packed structure of the struts.

The morphometric analysis of the CT data allowed to determine the cell size, struts thickness, ratio of the strut surface to the total volume, and the strut volume of the sample. The calculated results are shown in **Figure 6** and **Table 2**. The strut thickness results exhibit an almost Gaussian distribution for all foams evaluated. The average cell size and strut thickness (Table 2) were determined by applying a Gaussian approximation, accordingly. The samples are characterized by a slight change in the average value of the obtained results.

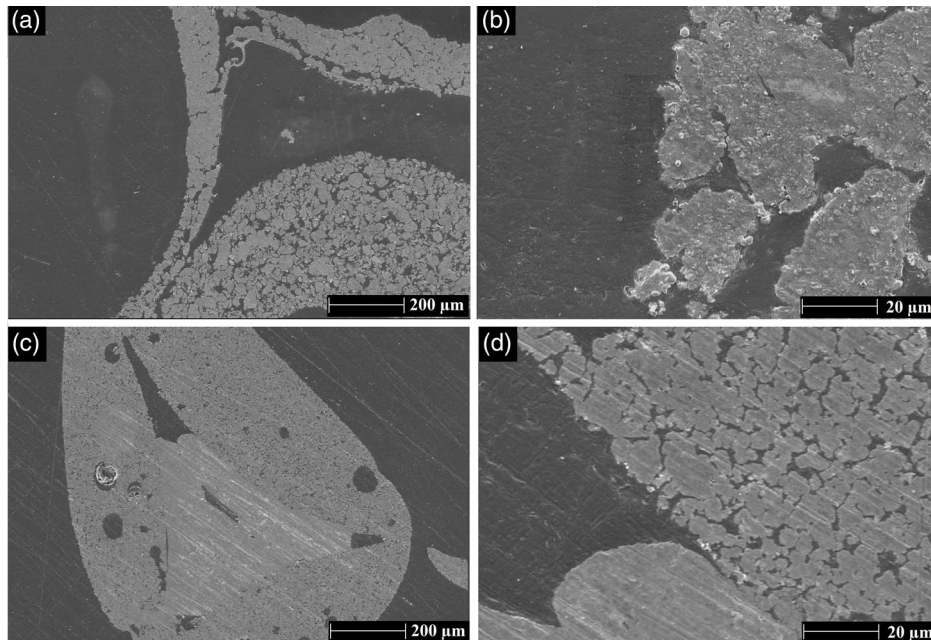


**Figure 5.** SEM images of the cross section of the foams made from the a,b) flaky, irregularly shaped Aldrich powder and c,d) dendritic near-spherical-shaped Ecka powder after heat treatment at 750 °C for 3 h.

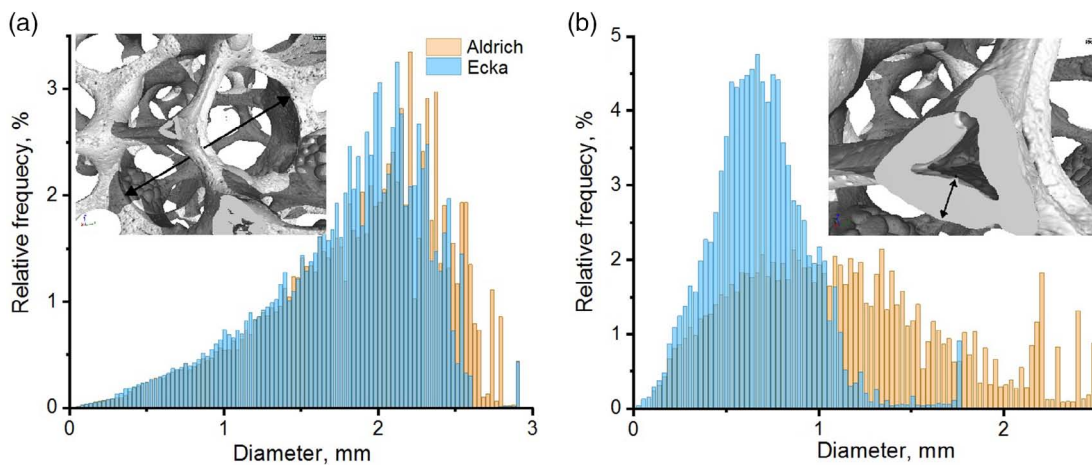


**Figure 6.** a) Cell size and b) strut thickness distribution calculated from a 3D  $\mu$ -CT reconstruction of aluminum foams made from the flaky, irregularly shaped Aldrich powder and spherical Ecka powder.

**Table 2.** Morphological data for the aluminum foams made from the flaky, irregularly shaped Aldrich powder and dendritic near-spherical-shaped Ecka powder after heat treatment at 750 °C for 3 h.

Powder	Cell size [mm]	Strut thickness [mm]	Strut surface/Total volume [mm <sup>-1</sup> ]	Strut surface/strut volume [mm <sup>-1</sup> ]
Flaky, irregularly shaped Aldrich powder foams	2.28 ± 0.26	0.99 ± 0.63	2.25	10.37
Spheroidal-shaped Ecka powder foams	2.12 ± 0.27	0.67 ± 0.24	2.99	10.66

The results of the XRD phase analyses are shown in **Figure 7**. The aluminum powders have an aluminum phase only as received from the supplier. Heat treatment of the Al foams in vacuum atmosphere leads to the formation of aluminum oxide

( $\alpha$ - and  $\gamma$ -Al<sub>2</sub>O<sub>3</sub>). The most intensive formation of aluminum oxide after heat treatment was observed for the foams made from the Aldrich powder. The oxide content is  $\approx$ 11.1% of  $\alpha$ -Al<sub>2</sub>O<sub>3</sub> and  $\approx$ 29.1% of  $\gamma$ -Al<sub>2</sub>O<sub>3</sub> in this sample. The oxide content in

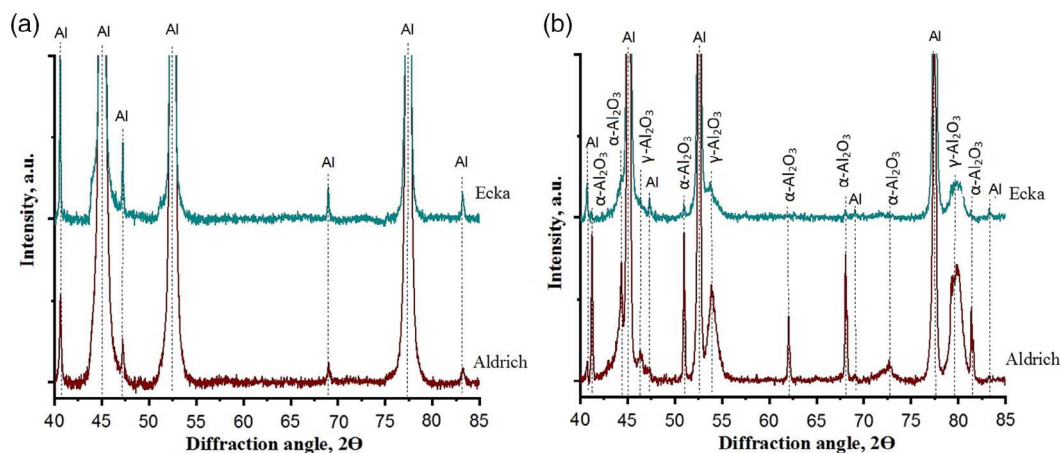


**Figure 7.** XRD curves of the flaky, irregularly shaped Aldrich powder (red curves) and spheroidal-shaped Ecka powder (green curves) a) before heat treatment and b) after heat treatment of the foams at 750 °C for 3 h.

the foams prepared from the Ecka powder is  $\approx 19.1\%$  of  $\gamma\text{-Al}_2\text{O}_3$ . The formation of traces of  $\alpha\text{-Al}_2\text{O}_3$  is observed, but the concentration is too low ( $\gg 1$  wt.%) to quantify it with the Rietveld technique.

The aluminum foams possess fairly the same total porosity, ranging between 90% and 91%, which is a precondition for a comparison of the compressive strength data; the results of the porosity and strength measurements of the foams are shown in **Table 3**. The total porosity includes material pores, cavities (hollow strut pores), and cell pores. The cell porosity relates to the foams without material pores and the hollow strut cavities. The total strut porosity consists of the hollow strut cavities and the material pores. The material porosity relates to closed and open material pores. The hollow strut porosity has cavities after PU template burnout, that was calculated from the volumetric shrinkage of the foams. From the Archimedes measurement, it follows that the heat treatment of aluminum foams made from the dendritic near-spherical-shaped Ecka powder has a less total strut ( $\approx 52\%$ ) and material porosity ( $\approx 40\%$ ) in comparison with the foams obtained from the flaky, irregularly shaped Aldrich powder under the same conditions ( $\approx 64.9\%$  and  $\approx 54.6\%$ , respectively). A similar behavior was observed in SEM investigations (Figure 5), where it is seen that the spheroidal-shaped Ecka powder particles are more densely packed (merged) after heat treatment.

The compressive strength shows the lowest values for the foams made from Aldrich powder ( $0.011 \pm 0.002$  MPa) (Table 3);

the compressive strength of the foams made from Ecka powder amounts to  $0.266 \pm 0.082$  MPa. The calculated Weibull parameter  $m$  for the compressive strength to each sample and sample series was  $\approx 6.8$  for the flaky, irregularly shaped Aldrich powder foams and  $\approx 3.2$  for the spheroidal-shaped Ecka powder foams.

#### 4. Discussion

Aluminum open-cell foams were heat treated at 750 °C, which is higher than the melting point of the used powders, but the obtained foams retained their shape. A possible explanation may be found with the coefficient of thermal expansion, which is four times higher for aluminum ( $27.4 \times 10^{-6} \text{ K}^{-1}$ ), compared with that of aluminum oxide ( $7.4 \times 10^{-6} \text{ °C}^{-1}$ ).<sup>[37]</sup> The thermal expansion difference can generate a stress on the oxide shell during heating, which is sufficient to disrupt the oxide shell around the powder particles. Simultaneously, oxide cracks healing appears with the process of the oxide shell rupture if oxygen is present in the heat-treatment furnace. Further heating up of the aluminum powders above the melting point leads to the disruption of the oxides by molten aluminum, which flows out of the surrounding shell.<sup>[16]</sup> As the result of the aforementioned tentative mechanism, the powder particles merge by the melting process, forming agglomerates of connected aluminum, formerly molten (Figure 5). The oxides are stable at the heat-treatment temperature of foams due to the melting point of aluminum oxide

**Table 3.** Total porosity, open strut porosity, and compressive strength of aluminum foams manufactured from the flaky, irregularly shaped Aldrich powder and spheroidal-shaped Ecka powder.

Powder	Total porosity <sup>a)</sup> [%]	Cell porosity <sup>b)</sup> [%]	Total strut porosity <sup>c)</sup> [%]	Material porosity [%]	Hollow strut porosity <sup>d)</sup> [%]	Compressive strength [MPa]
Flaky, irregularly shaped Aldrich powder foams	90.9	74.1	64.9	54.6	10.3	$0.011 \pm 0.002$
Spheroidal-shaped Ecka powder foams	90.3	79.5	52	40	12.3	$0.266 \pm 0.082$

<sup>a)</sup> $V_{\text{pores}}/V_{\text{foam}}$ ; <sup>b)</sup>Including the cavities after PU template burnout and material pores:  $(V_{\text{material}} + V_{\text{hollow strut pores}} + V_{\text{material pores}})/V_{\text{foam}}$ ; <sup>c)</sup>Related to the overall strut volume  $(V_{\text{hollow strut pores}} + V_{\text{material pores}})/(V_{\text{material}} + V_{\text{hollow strut pores}} + V_{\text{material pores}})$ ; <sup>d)</sup>The cavities after PU template burnout.

at  $\approx 2072^\circ\text{C}$ .<sup>[38]</sup> In this case, the oxide shells surrounding the particles behave like an oxidic skeleton in this system. This oxide network keeps the foam structure unchanged and is essential for the structural integrity of the foams and their stability.<sup>[16,39]</sup>

The frequency of the oxide shell breaking and healing might be higher for the irregular shaped powders. It was discussed in the study by Liu et al.<sup>[40]</sup> that any stress concentrations, occurring on the surface of the powders, induce oxide shell rupture. Therefore, a powder with less-regular shape has a higher frequency of the oxide shell rupture. In our case, it is the flaky, irregularly shaped Aldrich powder, which scavenges more oxygen (present as traces in the furnace) than the spheroidal-shaped Ecka powder. This behavior is consistent with the results from the TG and XRD investigations; it is evident from Figure 3 and 7 that the flaky, irregularly shaped Aldrich powder oxidized faster in comparison with the spheroidal-shaped Ecka powder; in the study by Patnaik,<sup>[38]</sup> a higher fracture rate of the oxide shell of the more irregular-shaped powder was observed.

The molten aluminum, flown out of the strut, is found unlike the foams from the flaky, irregularly shaped Aldrich powder after heat treatment of the foams manufactured from the spheroidal-shaped Ecka powder (Figure 5c). This behavior is explained by the lower oxidation rate of the spheroidal-shaped Ecka powder compared with the flaky, irregularly shaped Aldrich powder. In this case, the oxide shell on the surface of Ecka powder might be thinner compared with that of the Aldrich powder. Therefore, the molten aluminum easily disrupts the oxide shell, merging and flowing out of the strut.

The compressive test showed that the foams made from the spheroidal-shaped Ecka powder have a higher compressive strength which fits well to the denser-packed powder particles of the foam made from the Ecka powder (Table 3 and Figure 4 and 5). Therefore, formerly molten powder particles in this foam have better structural interconnectivity, stability, and strength than the metal foam made from the flaky, irregularly shaped Aldrich powder.

## 5. Conclusions

Open-cell aluminum foams were manufactured from 20 ppi PU templates by the sponge replication technique; two aluminum powders with different particle shapes and sizes were used. The open-cell green foams were treated in vacuum at  $750^\circ\text{C}$  and possess a total porosity of  $\approx 90\%$ . The microstructure of the foams is characterized by porous struts, resulting from incomplete heat treatment.

Particle size and shape of the starting aluminum powders play a critical role in the microstructure formation, phase content, porosity, and mechanical properties; open-cell aluminum foams manufactured from spheroidal-shaped powders ( $d_{50} = 6.6\ \mu\text{m}$ ) possess a denser structure and a lower level of strut porosity. This effect is assigned to the smaller surface area of this type of powder, and this results in a lower amount of aluminum oxide and a higher compressive strength compared with foams manufactured from flaky, irregularly shaped powders. Further research will be focused on the reduction of the amount of alumina.

## Acknowledgements

Financial support from the International Graduate School for Medical Engineering and Engineering Materials (MEMoRIAL) funded by the European Structural and Investment Funds (ESF) under the program "Sachsen-Anhalt WissenschaftInternationalisierung" is gratefully acknowledged. The authors are thankful to Katja Schelm and Dr. Iryna Smokovych for the TG and DSC investigations, Holger Voß for the XRD measurements (all OvGU-IWF), and Dr. Andreas Schlinkert (OvGU-MVT) for particle size measurements.

## Conflict of Interest

The authors declare no conflict of interest.

## Keywords

Al foams, porous materials, sponge replication techniques

Received: October 4, 2019

Revised: November 20, 2019

Published online: February 11, 2020

- [1] S. Singh, N. Bhatnagar, *J. Porous Mater.* **2018**, *25*, 537.
- [2] S. Kim, C. W. Lee, *Procedia Mater. Sci.* **2014**, *4*, 305.
- [3] F. García-Moreno, *Materials* **2016**, *9*, 85.
- [4] P. Quadbeck, K. Kümmel, R. Hauser, G. Standke, J. Adler, G. Stephani, in *Proc. CELLMAT 2010*, Dresden, Germany **2010**, p. 279.
- [5] B. Soni, S. Biswas, *Mater. Today: Proc.* **2015**, *2*, 1886.
- [6] Q. Li, N. J. Bjerrum, *J. Power Sources* **2002**, *110*, 1.
- [7] D. R. Egan, C. P. De León, R. J. K. Wood, R. L. Jones, K. R. Stokes, F. C. Walsh, *J. Power Sources* **2013**, *236*, 293.
- [8] Y. Liu, Q. Sun, W. Li, K. R. Adair, J. Li, X. Sun, *Green Energy Environ.* **2017**, *2*, 246.
- [9] P. Quadbeck, K. Kümmel, R. Hauser, G. Standke, J. Adler, G. Stephani, B. Kieback, *Adv. Eng. Mater.* **2011**, *13*, 1024.
- [10] J. Banhart, *MRS Bull.* **2003**, *28*, 290.
- [11] G. Zaragoza, R. Goodall, *Adv. Eng. Mater.* **2013**, *15*, 123.
- [12] X. Yang, Q. Hu, J. Du, T. Zou, J. Sha, C. He, N. Zhao, *Int. J. Fatigue* **2019**, *121*, 272.
- [13] L. Salvo, G. Martin, M. Suard, A. Marmottant, R. Dendievel, J. J. Blandin, *C. R. Phys.* **2014**, *15*, 662.
- [14] G. J. Davies, S. Zhen, *J. Mater. Sci.* **1983**, *18*, 1899.
- [15] A. Kennedy, *Porous Metals and Metal Foams Made from Powders, Powder Metallurgy*, InTech, London **2012**.
- [16] S. Barg, C. Soltmann, A. Schwab, D. Koch, W. Schwieger, G. Grathwohl, *J. Porous Mater.* **2011**, *18*, 89.
- [17] A. R. Jamaludin, S. R. Kasim, A. K. Ismail, M. Z. Abdullah, Z. A. Ahmad, *J. Eur. Ceram. Soc.* **2015**, *35*, 1905.
- [18] B. Dietrich, G. Schell, E. C. Bucharsky, R. Oberacker, M. J. Hoffmann, W. Schabel, H. Martin, *Int. J. Heat Mass Transfer* **2010**, *53*, 198.
- [19] K. Schwartzwalder, H. Somers, A. V. Somers, *US 3,090,094*, **1961**.
- [20] A. Choudhary, S. K. Pratihari, A. K. Agrawal, S. K. Behera, *Adv. Eng. Mater.* **2018**, *20*, 1700586.
- [21] H. I. Bakan, K. Korkmaz, *Mater. Des.* **2015**, *83*, 154.
- [22] C. Wang, H. Chen, X. Zhu, Z. Xiao, K. Zhang, X. Zhang, *Mater. Sci. Eng.* **2017**, *70*, 1192.
- [23] A. Manonukul, P. Srikudvien, M. Tange, *Mater. Sci. Eng.* **2016**, *650*, 432.
- [24] J. P. Li, S. H. Li, C. A. Van Blitterswijk, K. J. De Groot, *Biomed. Mater. Res., Part A* **2005**, *73*, 223.
- [25] H. I. Bakan, K. Korkmaz, *Mater. Des.* **2015**, *83*, 154.

- [26] E. Zaman, Ö. Keleş, *Acta Phys. Pol., A* **2014**, 125, 445.
- [27] C. Yagsi, O. Keles, in *Light Metals 2019*, Springer, Cham **2019**.
- [28] U. Betke, S. Dalicho, S. Rannabauer, A. Lieb, F. Scheffler, M. Scheffler, *Adv. Eng. Mater.* **2017**, 19, 1700138.
- [29] U. Betke, M. Klaus, J. G. Eggebrecht, M. Scheffler, A. Lieb, *Microporous Mesoporous Mater.* **2018**, 265, 43.
- [30] A. A. Coelho, *Topas Academic V5*, Coelho Software, Brisbane, Australia **2012**.
- [31] H. Henon, A. Alzina, J. Absi, D.S. Smith, *J. Porous Mater.* **2013**, 20, 37.
- [32] DIN EN, *Hochleistungskeramik; Monolithische Keramik; Allgemeine und strukturelle Eigenschaften; Teil 2: Bestimmung von Dichte und Porosität*, 623-2:1993-11, **2003**.
- [33] U. Betke, A. Lieb, F. Scheffler, M. Scheffler, *Adv. Eng. Mater.* **2017**, 19, 1600660.
- [34] S. W. Holman, R. R. Lawrence, L. Barr, *Proc. Am. Acad. Arts Sci.* **1895**, 31, 218.
- [35] H. Kwon, D. H. Park, Y. Park, J. F. Silvain, A. Kawasaki, Y. Park, *Met. Mater. Int.* **2010**, 16, 71.
- [36] M. A. Trunov, S. M. Umbrajkar, M. Schoenitz, J. T. Mang, E. L. Dreizin, *J. Phys. Chem. B* **2006**, 110, 13094.
- [37] C. A. Harper, *Ceramics, Glasses and Diamond: Handbook*, McGraw-Hill, New York **2001**.
- [38] P. Patnaik, *Inorganic Chemicals Handbook*, McGraw-Hill, New York **2002**.
- [39] C. Körner, M. Arnold, R. F. Singer, *Mater. Sci. Eng.* **2005**, 396, 28.
- [40] Z. Y. Liu, T. B. Sercombe, G. B. Schaffer, *Metall. Mater. Trans. A* **2007**, 38, 1351.